

Ferroelectricity in twisted double bilayer graphene

Renjun Du^{1,3}, Jingkuan Xiao^{1,3}, Di Zhang¹, Xiaofan Cai¹, Siqi Jiang¹, Fuzhuo Lian¹, Kenji Watanabe², Takashi Taniguchi², Lei Wang^{1,*} and Geliang Yu^{1,*}

¹ National Laboratory of Solid State Microstructures, School of Physics, Nanjing University, Nanjing 210093, China

² National Institute for Material Science, 1-1 Namiki, Tsukuba 305-0044, Japan

³ These authors contributed equally to this work.

* Authors to whom any correspondence should be addressed.

E-mail: leiwang@nju.edu.cn and yugeliang@nju.edu.cn

30 April 2024

Keywords: Twisted double bilayer graphene, ferroelectricity, moiré superlattice

Abstract.

Two-dimensional ferroelectrics can maintain vertical polarization up to room temperature, and are, therefore, promising for next-generation nonvolatile memories. Although natural two-dimensional ferroelectrics are few, moiré superlattices provide us with a generalized method to construct ferroelectrics from non-ferroelectric parent materials. We report a realization of ferroelectric hysteresis in a AB-BA stacked twisted double bilayer graphene (TDBG) system. The ferroelectric polarization is prominent at zero external displacement field and reduces upon increasing displacement fields. TDBG in the AB-BA configuration possesses a superlattice of non-centrosymmetric domains, exhibiting alternatively switchable polarities even without the assistance of any boron nitride layers; however, in the AB-AB stacking case, the development of polarized domains necessitates the presence of a second superlattice induced by the adjacent boron nitride layer. Therefore, twisted multilayer graphene systems offer us a fascinating field to explore two-dimensional ferroelectricity.

Submitted to: *2D Mater.*

1. Introduction

Ferroelectric materials possess a switchable electrical dipole moment that can be reversed by an external electrical field, enabling a wide range of applications in various areas, such as transducers, pyroelectric sensors, electrocaloric heat pumps, non-volatile memories and photovoltaic devices [1]. Its potential use in next-generation transistors with dense storage and low-power consumption instigates rapid developments in two-dimensional (2D) ferroelectrics. Despite thin-film ferroelectrics, van der Waals layered materials provide promising candidates for realizing 2D ferroelectrics with atomic thickness and intriguing properties [2, 3].

Natural van der Waals ferroelectrics with polar space groups are few [4–9], however constructing non-centrosymmetric structures with moiré superlattices open up new possibilities for designing unconventional ferroelectrics, expanding the family of 2D ferroelectric materials [10–15]. An array of domains with periodically alternating polarization can be created in moiré superlattices [16]. Applying an external electrical field can manipulate the polarity of domains, allowing the occurrence of ferroelectricity. This effect has been demonstrated in a variety of van der Waals materials, such as parallel-stacked hexagonal boron nitride (hBN) [17–20], twisted transition metal dichalcogenides (MoSe₂, WSe₂, MoS₂, and WS₂) homo- and hetero-structures [10, 21–24], and graphene-based superlattices [25–27]. Interlayer lattice sliding [10, 13, 20, 28] is found to well account for ferroelectric phenomena in twisted hBN and transition metal dichalcogenides; nevertheless, it is insufficient to explain the complex behaviour of ferroelectricity in bilayer-graphene-hBN superlattices, namely, layer-specific anomalous screening. Although the other scenarios considering correlated interactions [25, 27, 29] have been proposed, the real nature is still under discussion. On the other hand, in addition to realizing ferroelectricity in multi-element van der Waals materials, mixed-stacking graphite or twisted multilayer graphene offer us a novel system to achieve single-element ferroelectricity [30–33], which requires extensive experimental investigations.

Here, we present an experimental observation of ferroelectricity in a twisted double bilayer graphene system. We have constructed AB-BA stacked TDBG, which is anticipated to exhibit ferroelectricity as a result of the existence of symmetry-broken domains with opposite polarity. In addition, we have discussed the potential impact of the additional superlattice, induced by the adjacent hBN layer, on ferroelectricity. However, it is important to highlight that such additional superlattice is not a prerequisite for the generation of ferroelectricity in a twisted multilayer graphene system. Our experimental findings may improve the understanding of ferroelectricity in the intricate graphene-based superlattice system.

2. Results and discussions

We have fabricated a dual-gated device based on AB-BA stacked TDBG, as shown in figure 1(a). A ‘flip-and-stack’ approach [34] has been utilized to construct the AB-BA stacked double-bilayer graphene (see details in the supplemental material). We first picked up half of bilayer graphene (BLG) with a hBN flake affixed to a PDMS/PC (Polydimethylsiloxane/Poly(Bisphenol A carbonate)) stamp [35, 36], and then prepared the remaining part using the same procedure but with a second PDMS/PC stamp. The two stamps were brought into contact face-to-face by flipping one of them over. The twisted angle was controlled by carefully aligning the crystal axes of BLG under a high precision transfer set-up. The entire heterostructure (hBN-BLG-BLG-hBN) was picked up by the upper stamp and placed on a Si/SiO₂ substrate. The electrical field can be applied through a metallic top gate (Ti/Au) and a Si back gate. The sample was designed as a Hall bar and connected by depositing metallic edge contacts (Ti/Al/Au), as shown in figure 1(b). The device was measured at 1.6 K using a standard low-frequency lock-in technique.

Twisted double-bilayer graphene presents signatures of correlated interaction regardless of whether the stacking order is AB-AB or AB-BA [37–44]. Figure 1(c) shows the longitudinal resistivity ρ_{xx} of an AB-BA stacked TDBG device with a twist angle of 1.12° as a function of charge carrier densities n and displacement fields D . The charge carrier density is defined as $n = (C_{bg}V_{bg} + C_{tg}V_{tg})/e$, where C_{bg} (C_{tg}) is the capacitance between the back (top) gate and TDBG, and e is the elementary charge; and the external displacement field is obtained by $D = (C_{bg}V_{bg} - C_{tg}V_{tg})/2\epsilon_0$ (ϵ_0 is the vacuum permittivity), penetrating upward through the device. Unlike the previous works [37–44], there is no sign of a gap opening at the charge neutrality point (CNP), and the resistivity is decreased for higher D , implying the touching between the first conduction and valence bands. Although complete isolation of the flat bands is not realized, correlated states still appear on both electron and hole sides, resulting in a few resistance maxima at multiples of 1/4 filling of the flat bands. In contrast to earlier research [37–44], features of insulating states only exist on the hole side rather than the electron side, indicating that the bandwidth of the first valence band is narrower than that of the first conduction band. Usually, correlated states are symmetric for the variation of D in TDBG, but we found discernible asymmetric behaviours in resistivity, especially for $\nu = -1, -2, -3$. The occurrence of insulating states at $\nu = -1, -3$ and $D > 0.1$ V/nm originates from an additional superlattice between BLG and encapsulating BN which causes the nonequivalent dependence of the band structure on the direction of D [42]. For positive D , when the field penetrates from the bottom BLG to the top BLG, the hole density in the outer sheet of bottom BLG is higher; while it is suppressed for negative D (see figure 1(d)).

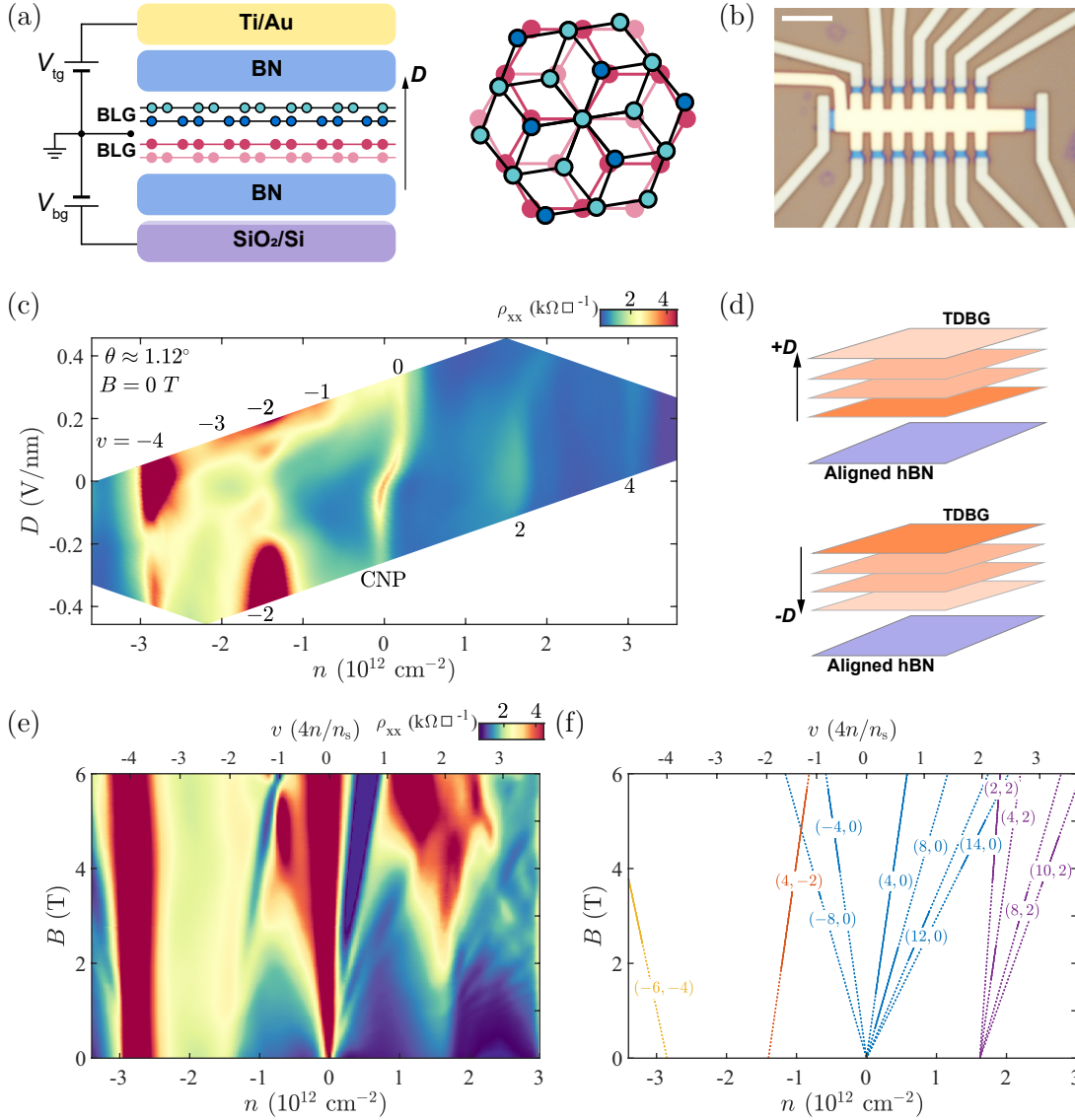


Figure 1. Twisted double bilayer graphene (sample S1). (a) Schematics of our dual-gated device made from twisted AB-BA stacked double bilayer graphene. (b) An optical image of the investigated device. The scale bar is $5 \mu\text{m}$. (c) Longitudinal resistivity measured by tuning charge carrier densities (n) and external displacement fields (D) at 1.6 K and zero magnetic field. Resistive maxima appear at the filling factors $\nu = 4n/n_s = -4, -3, -2, -1, 2, 4$ (n_s is the electron density of 4 electrons per moiré unit cell) and the charge neutrality points. (d) Schematics of the layer-resolved hole density for positive and negative D . (e) Landau fan diagram as a function of charge carrier densities and perpendicular magnetic fields at $D = 0$. (f) Schematics of the corresponding gapped states in (e). Different sets of Landau levels are grouped with distinct colors according to their intersections at $B = 0$.

Because the asymmetric features of correlated states at $\nu = -1, -3$ on the positive D side favour high-density states of holes, we can conclude that the bottom BN flake aligns with the bottom BLG layer. Nevertheless, the rotation angle between the bottom BN and BLG layers is relatively large ($\sim 5.6^\circ$) such that we didn't observe any associated resistivity peaks in transport measurements (see the alignment information in the supplemental material).

To explore the topological properties of the flat bands in AB-BA stacked TDBG, we investigated the evolution of resistivity in magnetic fields. Figure 1(d) shows a number of linearly dispersed Landau levels that are constituents of a Wannier diagram which is described by the Diophantine

equation $\nu = t\phi/\phi_0 + s$, where ν is the filling factor of electron density per Bloch band, ϕ is the magnetic flux per moiré unit cell, ϕ_0 is the magnetic flux quantum, t represents the quantized Hall conductivity $\sigma_{xy} = -te^2/h$, and s is the Bloch band filling at each gap. At $D = 0$, these Landau levels can be classified into two classes using topologically invariant integers (t, s) . For $s = 0, -4$ and $t \neq 0$, the Fermi level locates at the CNP or a single particle gap where the magneto-oscillations arise from integer quantum Hall effect. Around the CNP, the Landau levels take the sequence of $t = \pm 4, \pm 8, 12, 14$, presenting fourfold degeneracy as that in twisted bilayer graphene (TBG). Such lifting of eight-fold degeneracy in TBG may

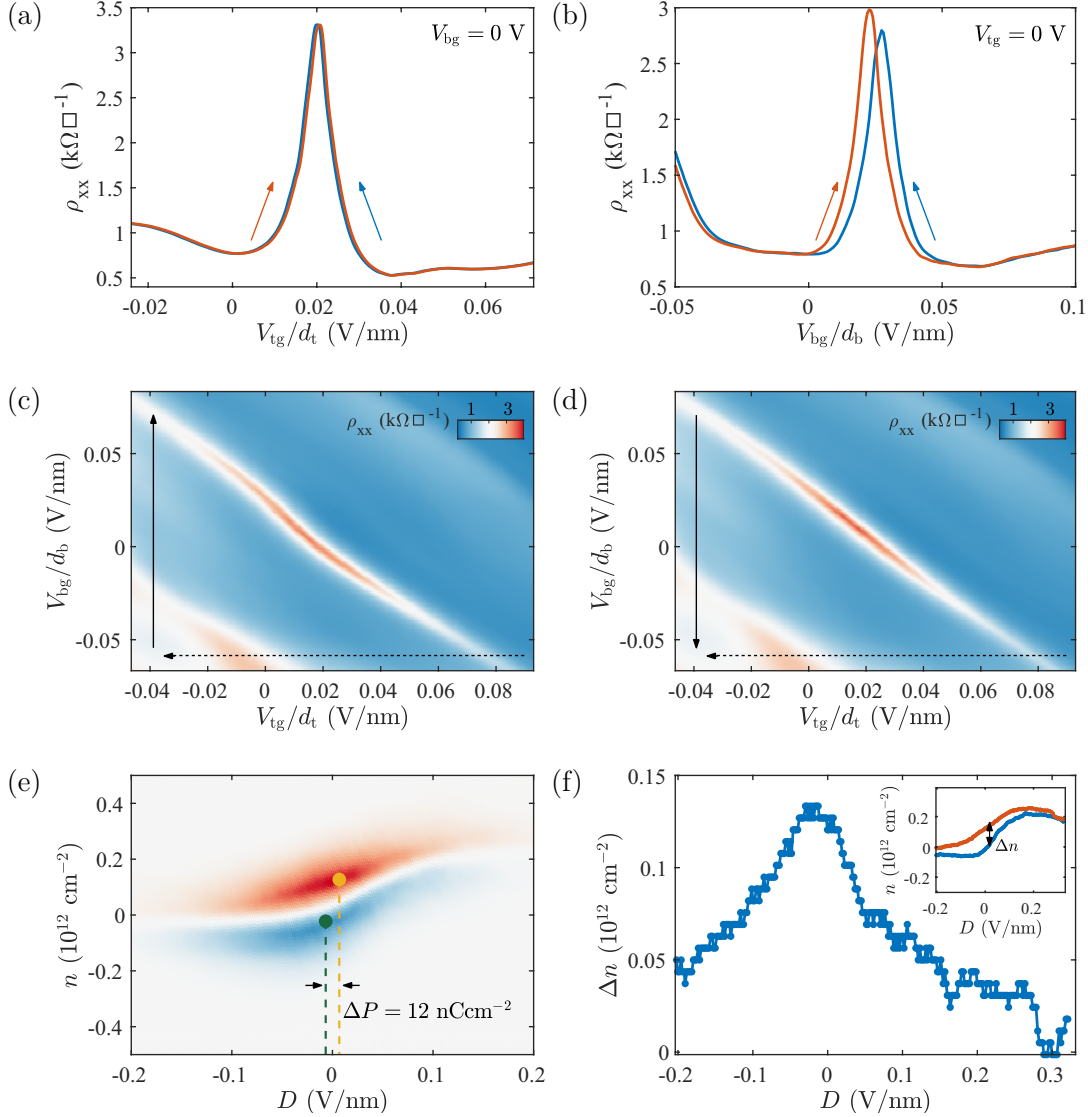


Figure 2. Ferroelectricity in AB-BA stacked twisted double bilayer graphene (sample S1). (a) Longitudinal resistivity shows no hysteresis for the forward (red curve) and backward (blue curve) scans of the top-gate voltage at $V_{bg} = 0$ V. (b) Ferroelectric hysteresis of the longitudinal resistivity occurs during sweeping the back-gate voltage forward (red curve) and backward (blue curve) at $V_{tg} = 0$. Here, the x -axis V_{tg} (V_{bg}) is normalized by the top (bottom) BN thickness d_t (d_b). In (c) and (d), the longitudinal resistivity is tuned by V_{tg} and V_{bg} together. We use V_{tg} as the fast scan axis and V_{bg} as the slow scan axis. The dashed and solid arrows denote the scan directions of V_{tg} and V_{bg} , respectively. The forward (c) and backward (d) scans of the back-gate voltage are shown separately. (e) The difference of longitudinal resistivity between the forward (c) and backward (d) resistivity maps, $\Delta\rho_{xx} = \rho_{xx}^{\text{forward}} - \rho_{xx}^{\text{backward}}$, as a function of charge carrier densities and external displacement fields. The green and yellow dots indicate two resistivity maxima of the charge neutrality points for the forward and backward sweeps, respectively. The remnant polarization is defined as $\Delta P = p^{\text{forward}} - p^{\text{backward}} = 12 \text{ nC} \cdot \text{cm}^{-2}$. (f) The difference in charge carrier densities (Δn) as a function of external displacement fields. Inset shows the positions of charge neutrality points in (c) and (d) with the red- and blue-dotted curves, respectively.

originate from C_3 symmetry broken[45–47]. In the case of TDBG, the number of degenerate states may also depend on stacking order. The AB-BA stacked TDBG lacks valley degeneracy while the AB-AB stacked TDBG preserves it even though these two configurations have nearly the same band structure at zero magnetic field[48]. Accordingly, the degeneracy of the Landau levels in AB-BA stacked TDBG is only half of that in the AB-AB case under weak magnetic fields. In the absence of triangle warping, the fourfold degeneracy in the AB-BA configuration may occur even

without considering other symmetry breaking[48]. On the other hand, states with integer $s = \pm 2$ and $t \neq 0$ correspond to correlated Chern insulators. The twofold degeneracy is found at $s = 2$ as the case in TBG[46, 47].

Apart from correlated states, the heterostructure of AB-BA stacked TDBG is also a fascinating system for the realization of ferroelectricity. A hysteretic behaviour of resistivity can be detected with the control of gate voltages. When we sweep the top gate forward (red curve) and backward (blue curve) while keeping $V_{bg} =$

0, the resistivity shows no lag between the two opposite sweeps (see figure 2(a)). However, a discernible hysteresis occurs when we tune the back-gate voltage forward and backward at $V_{\text{tg}} = 0$, implying ferroelectric polarization (see figure 2(b)). We use V_{tg} and V_{bg} as axes for the fast and slow scans, respectively, and then obtain two resistivity maps shown in figures 2(c) and (d) corresponding to the forward and backward sweeps of V_{bg} , respectively. The hysteresis is most apparent along the charge neutrality line that is bending with distinct curvatures for the forward and backward scans. The difference of resistivity between the forward- and backward-scan maps, *i. e.*, $\Delta\rho_{\text{xx}} = \rho_{\text{xx}}^{\text{forward}} - \rho_{\text{xx}}^{\text{backward}}$, is plotted as a function of D and n in figure 2(e). The ferroelectric polarization (P) generates an internal electrical field against the external field (D), leading to the resistivity maximum, originating from the band touching point, shifting from $D = 0$ to $D = -16.25\text{mV/nm}$ for the forward sweep (green dot) and to $D = 16.25\text{mV/nm}$ for the backward scan (yellow dot) [25]. The total shift (ΔD) between the two resistivity maxima illustrates the switchable remnant polarization, which can be defined as $\Delta P = \epsilon_0 \Delta D = 12\text{nC}\cdot\text{cm}^{-2}$. The ferroelectric polarization also causes a change in carrier density (Δn), leading to a lag of the CNP in ρ_{xx} (see figure 2(f)). Δn reduces with increasing $|D|$ and reaches its maximum at $D = 0$, indicating the largest polarization.

The motion of domains in moiré superlattices has been proven to play a significant role in the switch of ferroelectric polarization [10, 17, 18]. Here, we present evidence of this effect in AB-BA stacked TDBG. Figure 3(a) shows resistivity with more significant hysteresis that occurs not only at the CNP but also at the resistive peaks arising from correlated insulating states, implying the coexistence of ferroelectricity and strong correlations. Different scan rates have been used to demonstrate the stability of this large hysteresis. However, the hysteretic behaviour is eliminated to a great extent and limited in a small region around the CNP after we perform an electrical training process by tuning V_{bg} and V_{tg} together, as illustrated in figure 3(b). The remaining hysteresis is stable during measurements in the following months. We may ascribe this variation of hysteresis to the motion of domains facilitated by interlayer lattice sliding [10, 18, 50]. When tuning D with both gates, the polarization of domains can be changed, allowing a ferroelectric switch. If the domain wall is pinned around blisters, wrinkles, or defects, the switch of ferroelectricity is impeded, resulting in the reduction of hysteresis [10].

Interlayer lattice sliding is known to be a driving mechanism for the emergence of ferroelectricity [13, 16, 20, 28, 30, 51]. Creating moiré superlattices becomes a generalized approach to establish arrays of ferroelectric domains with switchable polarity. The structure of domains can be either centrosymmetric or non-centrosymmetric. For example, the stacking configurations in TDBG, such as ABAB and ABCA, are centrosymmetric and lack

polarity; while ABCB and ABAC are non-centrosymmetric and opposite in polarity (see figure 3(c)). Accordingly, sliding the domains from up-polarized to down-polarized or polarity to non-polarity can generate ferroelectricity. In the case of AB-BA stacked TDBG, a ferroelectric switch between ABCB and ABAC may exist, leading to the hysteretic behaviour of resistivity even without additional alignment of BN. Nevertheless, for AB-AB stacked TDBG, ferroelectricity can also be introduced by building an additional moiré structure using BN (see more data in the supplemental material), similar to the case in the BN-encapsulated bilayer graphene [25–27]. By adding the fifth layer of BN to TDBG (see the grey-shaded regions in figure 3(c)), the domains with all kinds of stacking order become non-centrosymmetric so that AB-AB stacked TDBG can also demonstrate ferroelectricity. In sample S1 with the AB-BA configuration, although bottom BN is aligned with TDBG by $\sim 5.6^\circ$, its effect on the formation of electrical dipoles might be weakened or even vanished [26] due to the small moiré wavelength of $\sim 2.5\text{nm}$. Interfacial lattice sliding provides a potential theoretical picture of ferroelectricity in TDBG without layer-specific-anomalous screening, even though distinct explanations [25, 27, 29], such as interaction-driven charge transfer, are still under discussion.

3. Conclusions

We have demonstrated the observation of ferroelectricity in AB-BA stacked TDBG assembled with a ‘flip-and-stack’ transfer method. Compared to TDBG with the AB-AB configuration, the AB-BA arranged TDBG exhibits similar band structures but with distinct topological properties, which may develop topologically non-trivial features in the Hofstadter spectrum, such as the lifting of valley degeneracy. On the other hand, TDBG with the AB-BA stacking also presents ferroelectricity as expected for the non-centrosymmetric domain structures, which is in sharp contrast to TDBG in the AB-AB case. In addition, the double moiré superlattices generated by BLG-BLG and BLG-hBN may contribute to the ferroelectric behaviour together by constructing five layer non-centrosymmetric domains. The role of moiré potential on ferroelectricity in graphene-based heterostructures is still under discussion. Our work provides new evidence which may improve the understanding of this phenomenon.

Acknowledgments

We thank A. S. Mayorov, G. Ma, Y. Han, P. Wang and J. Huang for their fruitful discussions. Financial support from the National Key R&D Program of China (Nos. 2018YFA0305804, 2018YFA0306800), the National Natural Science Foundation of China (Nos. 12004173, 11974169), the Natural Science Foundation of

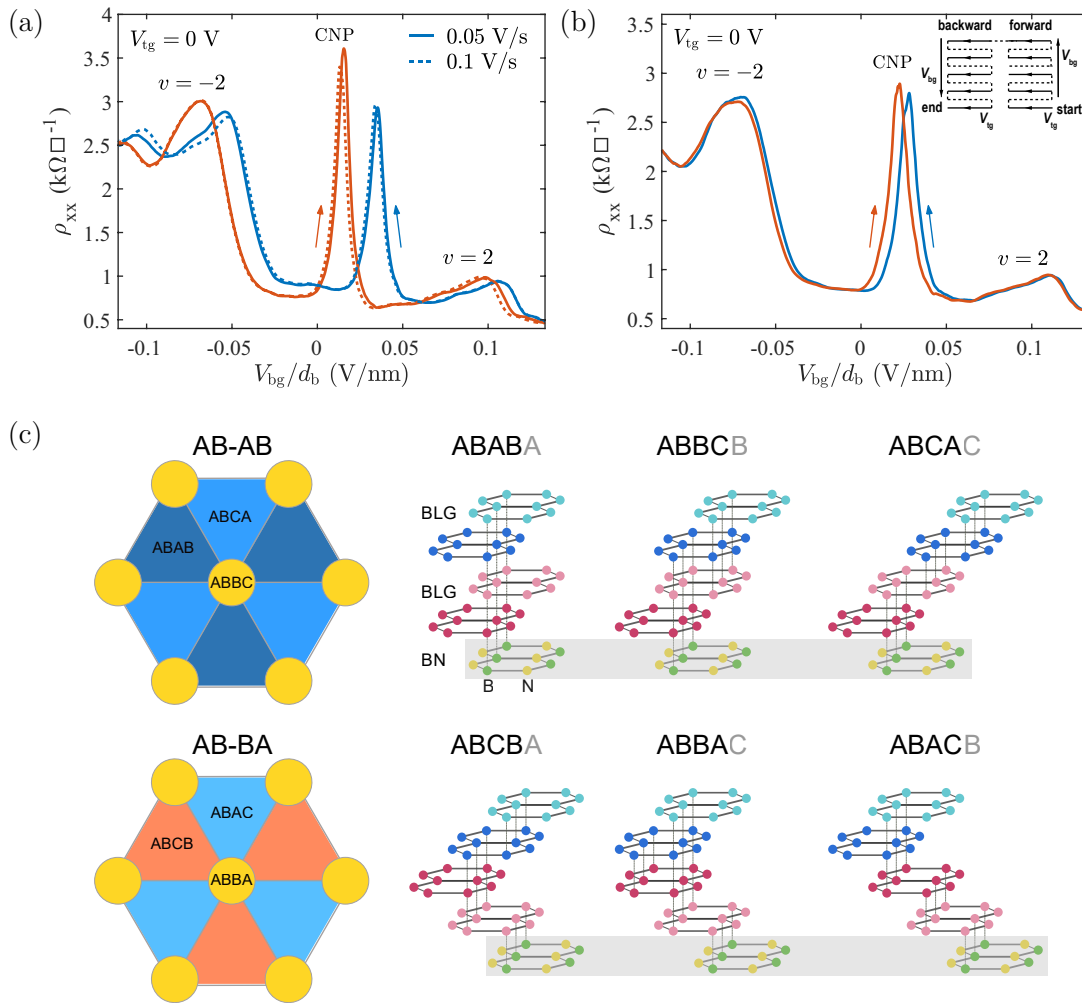


Figure 3. Ferroelectricity affected by the motion of domains (sample S1). (a) Longitudinal resistivity measured by sweeping the back-gate voltage forward (red) and backward (blue) at $V_{fg} = 0$. The dashed and solid lines denote scans with the fast- and slow-scan rates, respectively. The hysteresis is shown at both the charge neutrality point and half-filling positions. (b) Longitudinal resistivity measured with respect to V_{bg} at $V_{fg} = 0$ after a sequential manipulation of both top- and back-gate voltages. The black zigzag lines describe the sequence of the electrical training process. A reduction of hysteresis is observed. (c) Schematics of the stacking order of domains in the AB-AB and AB-BA stacked TDBG superlattices. In the case of AB-AB stacked TDBG, the domains present three types of centrosymmetric stacking order, that is ABAB, ABBC, and ABCA, which can become non-centrosymmetric by adding a superlattice using an adjacent BN lattice (grey-shaded region). The structures for the five-layer domains change to ABABA, ABBCB and ABCAC with the boron atom sitting below the carbon atom, which is energetically favourable [28, 49]. For the AB-BA stacked TDBG, it shows three non-centrosymmetric domains with ABCB, ABBA, and ABAC stacking, which give rise to a lattice with alternating polarized domains (up-polarized ABCB and down-polarized ABAC). When adding a superlattice with BN, the domains are still non-centrosymmetric, taking the stacking structures of ABCBA, ABBAC, and ABACB.

Jiangsu Province (Nos. BK20220066), and the Fundamental Research Funds for the Central Universities (Nos. 020414380087, 020414913201) are gratefully acknowledged.

References

- [1] Martin L W and Rappe A M 2016 Thin-film ferroelectric materials and their applications *Nat. Rev. Mater.* **2** 16087
- [2] Wang C, You L, Cobden D and Wang J 2023 Towards two-dimensional van der Waals ferroelectrics *Nat. Mater.* **22** 542–552
- [3] Zhang D, Schoenherr P, Sharma P and Seidel J 2023 Ferroelectric order in van der Waals layered materials *Nat. Rev. Mater.* **8** 25–40
- [4] Liu F, You L, Seyler K L, Li X, Yu P, Lin J, Wang X, Zhou J, Wang H, He H, Pantelides S T, Zhou W, Sharma P, Xu X, Ajayan P M, Wang J and Liu Z 2016 Room-temperature ferroelectricity in CuInP_2S_6 ultrathin flakes *Nat. Commun.* **7** 12357
- [5] Fei Z, Zhao W, Palomaki T A, Sun B, Miller M K, Zhao Z, Yan J, Xu X and Cobden D H 2018

- Ferroelectric switching of a two-dimensional metal *Nature* **560** 336–339
- [6] Yuan S, Luo X, Chan H L, Xiao C, Dai Y, Xie M and Hao J 2019 Room-temperature ferroelectricity in MoTe₂ down to the atomic monolayer limit *Nat. Commun.* **10** 1775
- [7] Cui C, Hu W J, Yan X, Addiego C, Gao W, Wang Y, Wang Z, Li L, Cheng Y, Li P, Zhang X, Alshareef H N, Wu T, Zhu W, Pan X and Li L J 2018 Intercorrelated in-plane and out-of-plane ferroelectricity in ultrathin two-dimensional layered semiconductor In₂Se₃ *Nano Lett.* **18** 1253–1258
- [8] Zhou Y, Wu D, Zhu Y, Cho Y, He Q, Yang X, Herrera K, Chu Z, Han Y, Downer M C, Peng H and Lai K 2017 Out-of-plane piezoelectricity and ferroelectricity in layered α -In₂Se₃ nanoflakes *Nano Lett.* **17** 5508–5513
- [9] Xiao J, Wang Y, Wang H, Pemmaraju C D, Wang S, Muscher P, Sie E J, Nyby C M, Devereaux T P, Qian X, Zhang X and Lindenberg A M 2020 Berry curvature memory through electrically driven stacking transitions *Nat. Phys.* **16** 1028–1034
- [10] Weston A, Castanon E G, Enaldiev V, Ferreira F, Bhattacharjee S, Xu S, Corte-León H, Wu Z, Clark N, Summerfield A, Hashimoto T, Gao Y, Wang W, Hamer M, Read H, Fumagalli L, Kretinin A V, Haigh S J, Kazakova O, Geim A K, Fal'ko V I and Gorbachev R 2022 Interfacial ferroelectricity in marginally twisted 2D semiconductors *Nat. Nanotechnol.* **17** 390–395
- [11] Magorrian S J, Enaldiev V V, Zólyomi V, Ferreira F, Fal'ko V I and Ruiz-Tijerina D A 2021 Multifaceted moiré superlattice physics in twisted WSe₂ bilayers *Phys. Rev. B* **104**(12) 125440
- [12] Enaldiev V V, Ferreira F, Magorrian S J and Fal'ko V I 2021 Piezoelectric networks and ferroelectric domains in twistrionic superlattices in WS₂/MoS₂ and WSe₂/MoSe₂ bilayers *2D Mater.* **8** 025030
- [13] Li L and Wu M 2017 Binary compound bilayer and multilayer with vertical polarizations: Two-dimensional ferroelectrics, multiferroics, and nanogenerators *ACS Nano* **11** 6382–6388
- [14] Zhao P, Xiao C and Yao W 2021 Universal superlattice potential for 2D materials from twisted interface inside h-BN substrate *npj 2D Mater. Appl.* **5** 38
- [15] Zhang Y, Yuan N F Q and Fu L 2020 Moiré quantum chemistry: Charge transfer in transition metal dichalcogenide superlattices *Phys. Rev. B* **102**(20) 201115
- [16] Enaldiev V V, Ferreira F and Fal'ko V I 2022 A scalable network model for electrically tunable ferroelectric domain structure in twistrionic bilayers of two-dimensional semiconductors *Nano Lett.* **22** 1534–1540
- [17] Yasuda K, Wang X, Watanabe K, Taniguchi T and Jarillo-Herrero P 2021 Stacking-engineered ferroelectricity in bilayer boron nitride *Science* **372** 1458–1462
- [18] Woods C R, Ares P, Nevison-Andrews H, Holwill M J, Fabregas R, Guinea F, Geim A K, Novoselov K S, Walet N R and Fumagalli L 2021 Charge-polarized interfacial superlattices in marginally twisted hexagonal boron nitride *Nat. Commun.* **12** 347
- [19] Fraunié J, Jamil R, Kantelberg R, Petit L, Lepleux E, Pacheco L, Watanabe K, Taniguchi T, Jacques V, Lombez L, Lassagne B, Marie X and Robert C 2023 Gate-free doping of a 2D semiconductor using ferroelectric hexagonal boron nitride interface *arXiv preprint arXiv:2307.08146*
- [20] Stern M V, Waschitz Y, Cao W, Nevo I, Watanabe K, Taniguchi T, Sela E, Urbakh M, Hod O and Shalom M B 2021 Interfacial ferroelectricity by van der Waals sliding *Science* **372** 1462–1466
- [21] Wang X, Yasuda K, Zhang Y, Liu S, Watanabe K, Taniguchi T, Hone J, Fu L and Jarillo-Herrero P 2022 Interfacial ferroelectricity in rhombohedral-stacked bilayer transition metal dichalcogenides *Nat. Nanotechnol.* **17** 367–371
- [22] An L, Zhou Z, Feng X, Huang M, Cai X, Chen Y, Zhao P, Dai X, Zhang J, Yao W, Liu J and Wang N 2023 Unconventional ferroelectricity in half-filling states of antiparallel stacking of twisted WSe₂ *arXiv preprint arXiv:2301.02025*
- [23] Deb S, Cao W, Raab N, Watanabe K, Taniguchi T, Goldstein M, Kronik L, Urbakh M, Hod O and Ben Shalom M 2022 Cumulative polarization in conductive interfacial ferroelectrics *Nature* **612** 465–469
- [24] Rogée L, Wang L, Zhang Y, Cai S, Wang P, Chhowalla M, Ji W and Lau S P 2022 Ferroelectricity in untwisted heterobilayers of transition metal dichalcogenides *Science* **376** 973–978
- [25] Zheng Z, Ma Q, Bi Z, de la Barrera S, Liu M H, Mao N, Zhang Y, Kiper N, Watanabe K, Taniguchi T, Kong J, Tisdale W A, Ashoori R, Gedik N, Fu L, Xu S Y and Jarillo-Herrero P 2020 Unconventional ferroelectricity in moiré heterostructures *Nature* **588** 71–76
- [26] Niu R, Li Z, Han X, Qu Z, Ding D, Wang Z, Liu Q, Liu T, Han C, Watanabe K, Taniguchi T, Wu M, Ren Q, Wang X, Hong J, Mao J, Han Z, Liu K, Gan Z and Lu J 2022 Giant ferroelectric polarization in a bilayer graphene heterostructure *Nat. Commun.* **13** 6241
- [27] Zheng Z, Wang X, Zhu Z, Carr S, Devakul T, de la Barrera S, Paul N, Huang Z, Gao A, Zhang Y, Bérubé D, Evancho K N, Watanabe K, Taniguchi T, Fu L, Wang Y, Xu S Y, Kaxiras E, Jarillo-Herrero P and Ma Q 2023 Electronic ratchet effect in a moiré system:

- signatures of excitonic ferroelectricity *arXiv preprint arXiv:2306.03922*
- [28] Yang L and Wu M 2023 Across-layer sliding ferroelectricity in 2D heterolayers *Adv. Funct. Mater.* **33** 2301105
- [29] Zhu Z, Carr S, Ma Q and Kaxiras E 2022 Electric field tunable layer polarization in graphene/boron-nitride twisted quadrilayer superlattices *Phys. Rev. B* **106**(20) 205134
- [30] Garcia-Ruiz A, Enaldiev V, McEllistim A and Fal'ko V I 2023 Mixed-stacking few-layer graphene as an elemental weak ferroelectric material *Nano Lett.* **23** 4120–4125
- [31] Yang L, Ding S, Gao J and Wu M 2023 Atypical sliding and moiré ferroelectricity in pure multilayer graphene *arXiv preprint arXiv:2305.07286*
- [32] Atri S S, Cao W, Alon B, Roy N, Stern M V, Fal'ko V, Goldstein M, Kronik L, Urbakh M, Hod O and Shalom M B 2023 Spontaneous electric polarization in graphene polytypes *arXiv preprint arXiv:2305.10890*
- [33] Winterer F, Geisenhof F R, Fernandez N, Seiler A M, Zhang F and Weitz R T 2023 Ferroelectric and anomalous quantum Hall states in bare rhombohedral trilayer graphene *arXiv preprint arXiv:2305.04950*
- [34] Yang Y, Li J, Yin J, Xu S, Mullan C, Taniguchi T, Watanabe K, Geim A K, Novoselov K S and Mishchenko A 2020 In situ manipulation of van der Waals heterostructures for twistronics *Sci. Adv.* **6** eabd3655
- [35] Kim K, Yankowitz M, Fallahazad B, Kang S, Movva H C P, Huang S, Larentis S, Corbet Chris M and Taniguchi T, Watanabe K, Banerjee S K, LeRoy B J and Tutuc E 2016 van der Waals heterostructures with high accuracy rotational alignment *Nano Lett.* **16** 1989–1995
- [36] Cao Y, Luo J Y, Fatemi V, Fang S, Sanchez-Yamagishi J D, Watanabe K, Taniguchi T, Kaxiras E and Jarillo-Herrero P 2016 Superlattice-induced insulating states and valley-protected orbits in twisted bilayer graphene *Phys. Rev. Lett.* **117**(11) 116804
- [37] Cao Y, Rodan-Legrain D, Rubies-Bigorda O, Park J M, Watanabe K, Taniguchi T and Jarillo-Herrero P 2020 Tunable correlated states and spin-polarized phases in twisted bilayer–bilayer graphene *Nature* **583** 215–220
- [38] He M, Li Y, Cai J, Liu Y, Watanabe K, Taniguchi T, Xu X and Yankowitz M 2021 Symmetry breaking in twisted double bilayer graphene *Nat. Phys.* **17** 26–30
- [39] Burg G W, Zhu J, Taniguchi T, Watanabe K, MacDonald A H and Tutuc E 2019 Correlated insulating states in twisted double bilayer graphene *Phys. Rev. Lett.* **123**(19) 197702
- [40] Liu X, Hao Z, Khalaf E, Lee J Y, Ronen Y, Yoo H, Haei Najafabadi D, Watanabe K, Taniguchi T, Vishwanath A and Kim P 2020 Tunable spin-polarized correlated states in twisted double bilayer graphene *Nature* **583** 221–225
- [41] Shen C, Chu Y, Wu Q, Li N, Wang S, Zhao Y, Tang J, Liu J, Tian J, Watanabe K, Taniguchi T, Yang R, Meng Z Y, Shi D, Yazyev O V and Zhang G 2020 Correlated states in twisted double bilayer graphene *Nat. Phys.* **16** 520–525
- [42] He M, Cai J, Zhang Y H, Liu Y, Li Y, Taniguchi T, Watanabe K, Cobden D H, Yankowitz M and Xu X 2021 Chirality-dependent topological states in twisted double bilayer graphene *arXiv preprint arXiv:2109.08255*
- [43] Wang Y, Herzog-Arbeitman J, Burg G W, Zhu J, Watanabe K, Taniguchi T, MacDonald A H, Bernevig B A and Tutuc E 2022 Bulk and edge properties of twisted double bilayer graphene *Nat. Phys.* **18** 48–53
- [44] Kouri M, Coleman C, Gao Z, Vishnuradhan A, Watanabe K, Taniguchi T, Zhu J, MacDonald A H and Folk J 2022 Spontaneous time-reversal symmetry breaking in twisted double bilayer graphene *Nat. Commun.* **13** 6468
- [45] Zhang Y H, Po H C and Senthil T 2019 Landau level degeneracy in twisted bilayer graphene: Role of symmetry breaking *Phys. Rev. B* **100**(12) 125104
- [46] Saito Y, Ge J, Rademaker L, Watanabe K, Taniguchi T, Abanin D A and Young A F 2021 Hofstadter subband ferromagnetism and symmetry-broken Chern insulators in twisted bilayer graphene *Nat. Phys.* **17** 478–481
- [47] Yu J, Foutty B A, Han Z, Barber M E, Schattner Y, Watanabe K, Taniguchi T, Phillips P, Shen Z X, Kivelson S A and Feldman B E 2022 Correlated Hofstadter spectrum and flavour phase diagram in magic-angle twisted bilayer graphene *Nat. Phys.* **18** 825–831
- [48] Crosse J A, Nakatsuji N, Koshino M and Moon P 2020 Hofstadter butterfly and the quantum Hall effect in twisted double bilayer graphene *Phys. Rev. B* **102**(3) 035421
- [49] Moore S L, Ciccarino C J, Halbertal D, McGilly L J, Finney N R, Yao K, Shao Y, Ni G, Sternbach A, Telford E J, Kim B S, Rossi S E, Watanabe K, Taniguchi T, Pasupathy A N, Dean C R, Hone J, Schuck P J, Narang P and Basov D N 2021 Nanoscale lattice dynamics in hexagonal boron nitride moiré superlattices *Nat. Commun.* **12** 5741
- [50] Zhang S, Xu Q, Hou Y, Song A, Ma Y, Gao L, Zhu M, Ma T, Liu L, Feng X Q and Li Q 2022 Domino-like stacking order switching in twisted monolayer–multilayer graphene *Nat. Mater.* **21** 621–626

- [51] Molino L, Aggarwal L, Enaldiev V, Plumadore R, I Fal'ko V and Luican-Mayer A 2023 Ferroelectric switching at symmetry-broken interfaces by local control of dislocations networks *Adv. Mater.* 2207816